Search for colour reconnection effects in $e^+e^- \to W^+W^- \to$ hadrons through particle-flow studies at LEP

P. Achard, O. Adriani, M. Aguilar-Benitez, J. Alcaraz, G. Alemanni, J. Allaby, A. Aloisio, M.G. Alviggi, H. Anderhub, V.P. Andreev, et al.

EUROPEAN ORGANIZATION FOR NUCLEAR RESEARCH

CERN-EP/2003-012
March 13, 2003

Search for Colour Reconnection Effects in $e^+e^- \to W^+W^- \to$ hadrons through Particle-Flow Studies at LEP

The L3 Collaboration

Abstract

A search for colour reconnection effects in hadronic decays of W pairs is performed with the L3 detector at centre-of-mass energies between 189 and 209 GeV. The analysis is based on the study of the particle flow between jets associated to the same W boson and between two different W bosons in $q\bar{q}q\bar{q}$ events. The ratio of particle yields in the different interjet regions is found to be sensitive to colour reconnection effects implemented in some hadronisation models. The data are compared to different models with and without such effects. An extreme scenario of colour reconnection is ruled out.

Submitted to *Phys. Lett. B*

1 Introduction

According to the string model of hadronisation, the particles produced in the process $e^+e^- \to W^+W^- \to$ *hadrons* originate, in the absence of colour reconnection, from the fragmentation of two colour singlet strings each of which is stretched between the two quarks from a W boson. In this case the hadrons are uniquely associated to a particular W and there is a direct correspondence between the jets formed by these hadrons and the primary quarks from the W boson decays. Energy-momentum is separately conserved for each of the W systems. However, it has been suggested that interactions may occur between the decay products of the two W bosons [1, 2, 3, 4]. The main justification for this "cross-talk" is the relatively short distance separating the decay vertices of the W bosons produced in e^+e^- annihilation (≈ 0.1 fm) compared to the typical hadronic scale (1 fm), which implies a large space-time overlap of the two hadronising systems.

The main consequence of these interactions, called Colour Reconnection (CR) effects, is a modification of the distribution in phase space of hadrons. CR effects are thought to be suppressed in the hard perturbative phase, but may be more important in the soft gluon emission regime [2]. While hard gluons, with energy greater than the W width, are radiated independently from different colour singlets, soft gluons could in principle be affected by the colour strings of both decaying W's. Such CR would affect the number of soft particles in specific phase space regions, especially outside the jet cores.

The study of CR is interesting not only for probing QCD dynamics but also for determining a possible bias in the W mass measurement in the four-quark channel. CR could affect the invariant masses of jet pairs originating from W decays. Therefore the precision with which the W mass may be determined using the four-quark channel depends strongly on the understanding of CR effects. Events where only one W decays hadronically are unaffected by CR.

Previous LEP studies of CR, performed at centre-of-mass energy $\sqrt{s} \leq 183$ GeV, were based on charged particle multiplicity and momentum distributions [5].

The analysis presented in this paper uses the method suggested in Reference 6 based on energy and particle flow to probe the string topology of four-quark events to search for particular effects of particle depletion and enhancement. The results are based on 627 pb^{-1} of data collected with the L3 detector [7] at $\sqrt{s}$=189−209 GeV. Comparisons with various models are made at detector level and the compatibility with the existence of CR effects in various models is investigated.

2 Colour Reconnection Models

Several phenomenological models have been proposed [2, 3, 8, 9, 10, 11] to describe CR effects in $e^+e^- \to W^+W^- \to$ *hadrons* events. The analysis presented in this paper is performed with some of those CR models, which are implemented in the PYTHIA [12], ARIADNE [13] and HERWIG [14] Monte Carlo (MC) programs.

We investigate two models by Sjöstrand and Khoze [2] implemented in PYTHIA. They are based on rearrangement of the string configuration during the fragmentation process. They follow the space-time evolution of the strings and allow local reconnections if the strings overlap or cross, depending on the string definition (elongated bags or vortex lines).

In the type I model (SKI) the strings are associated with colour flux tubes having a significant transverse extension. The reconnection occurs when these tubes overlap and only one reconnection is allowed, the one with the largest overlap volume. The reconnection probability

depends on this volume of overlap and is controlled by one free parameter, $k_{\rm I}$, which can be varied in the model to generate event samples with different fractions of reconnected events. The relation with the event reconnection probability ($P_{\rm reco}$) is given by the following formula:

$$P_{\rm reco} = 1 - \exp(-f k_{\rm I}) \tag{1}$$

where f is a function of the overlap volume of the two strings, which depends on W-pair kinematics varying with $\sqrt{s}$. The default value of $k_{\rm I}$ is 0.6 [2], which corresponds to a reconnection probability of about 30% at $\sqrt{s}$=189 GeV. This analysis is performed with three different values of $k_{\rm I}$: 0.6, 3 and 1000, corresponding to reconnection probabilities at $\sqrt{s}$=189 GeV of about 30%, 66% and nearly 100%, respectively.

In the type II model (SKII) the strings have no lateral extent and the reconnection occurs, with unit probability, when they cross. The fraction of reconnected events in this model is of the order of 30% at $\sqrt{s}$=189 GeV.

The CR model implemented in ARIADNE is based on reconnection of coloured dipoles before the string fragmentation takes place [9]. In the AR2 scheme, which is investigated here, reconnections are allowed if they reduce the string length. While reconnections within a W are allowed at all scales, those between W's are only allowed after the parton showers have evolved down to gluon energies less than 2 GeV. At $\sqrt{s}$ =189 GeV they affect about 55% of the events.

The CR scheme implemented in HERWIG is, as for the string fragmentation, a local phenomenon since the cluster fragmentation process follows the space-time development. In this model [10] the clusters are rearranged if their space-time extension is reduced. This rearrangement occurs with a probability equal to $1/N^2_{\rm colour}$, with default value $N_{\rm colour} = 3$, giving about 23% of reconnected events.

All probabilities discussed above are derived as fraction of events where at least one reconnection occurs either within the same W or between two W's.

3 Event Selection

The energy measured in the electromagnetic and hadronic calorimeters and in the tracking chamber is used to select $\rm e^+e^- \to W^+W^- \to$ *hadrons* events. The total visible energy ($E_{\rm vis}$) and the energy imbalance parallel ($E_\parallel$) and perpendicular ($E_\perp$) to the beam direction are measured. The number of clusters, defined as objects obtained from a non-linear combination of charged tracks with a transverse momentum greater than 100 MeV and calorimetric clusters with a minimum energy of 100 MeV, is denoted by $N_{\rm cluster}$. The selection criteria are:

$$E_{\rm vis}/\sqrt{s} > 0.7; \qquad E_\perp/E_{\rm vis} < 0.2; \qquad |E_\parallel|/E_{\rm vis} < 0.2; \qquad N_{\rm cluster} \geq 40.$$

In addition the events must have 4 jets reconstructed with the Durham algorithm [15] with $y_{\rm cut} = 0.01$. To reduce the contamination from semileptonic W decays, events with energetic μ or e are rejected. Events with hard initial state radiation (ISR) are rejected as described in Reference 16. Additional criteria select events with nearly perfect quark-jet association, necessary for the study of particle and energy flow between jets. The two largest interjet angles are required to be between 100° and 140° and not adjacent. The two other interjet angles must be less than 100°. This selection guarantees similar sharing of energy between the four primary partons with the two strings evolving back-to-back and similar interjet regions between the two W's. The above cuts are optimized by studying MC $\rm W^+W^-$ events at $\sqrt{s}$=189 GeV using the KORALW [17] MC generator interfaced with the PYTHIA fragmentation model without CR.

Relaxing the angular criteria increases the efficiency but gives lower probability to have correct W-jet pairing due to the more complicated event topology.

The number of selected events, the number of expected events, the selection efficiency and the percentage of correct pairing are given in Table 1. After applying all the cuts the full sample contains 666 events with an average efficiency of 12% and a purity of about 85% for $e^+e^- \to W^+W^- \to hadrons$. The average probability to have the correct pairing between the W bosons and their associated jets is estimated to be 91%.

The background is composed of $q\bar{q}(\gamma)$ events and Z-pair production events, in similar amounts. Background from semileptonic W pair decays is found to be negligible (less than 0.3%). The $q\bar{q}(\gamma)$ process is modeled with the KK2F MC program [18], interfaced with JETSET [19] routines to describe the QCD processes, and the background from Z-pair production is simulated with PYTHIA. For CR studies W-pair events are simulated with PYTHIA. All MC samples are passed through a realistic detector simulation [20] which takes into account time dependent detector effects and inefficiencies.

4 Particle- and Energy-Flow Distributions

The algorithm to build the particle- and energy-flow distributions [6] (Figure 1) starts by defining the plane spanned by the most energetic jet (jet 1) and the closest jet making an angle with jet 1 greater than 100° which is most likely associated to the same W (jet 2). For each event, the momentum vector direction of each particle is then projected on to this plane. The particle and energy flows are measured as a function of the angle, ϕ, between jet 1 and the projected momentum vector for the particles located between jets 1 and 2. In order to take into account the fact that the W-pair events are not planar a new plane is defined for each remaining pair of adjacent jets. In this four-plane configuration the angle ϕ is defined as increasing from jet 1 toward jet 2, then to the closest jet from the other W (jet 3) toward the remaining jet (jet 4) and back to jet 1. The angle $\phi_{j,i}$ of a particle i having a projected momentum vector located between jets j and $j+1$ is calculated in the plane spanned by these two jets. A particle i making an angle ϕ_i with respect to jet 1 adds an entry equal to 1 in the particle-flow distribution and adds an entry equal to its energy, normalised to the total event energy, in the energy-flow distribution for the corresponding ϕ bin.

The distributions are calculated using, for the particle definition, the clusters defined in the previous section.

Figure 2 shows the particle- and energy-flow distributions obtained for the data and the MC predictions at detector level by using only the first plane for projecting all the particles. The data and MC distributions agree over the full angular range in both cases.

In order to compare the interjet regions the angles in the planes are rescaled by the angle between the two closest jets. For a particle i located between jets j and $j+1$ the rescaled angle is

$$\phi_i^{\mathrm{resc}} = j - 1 + \frac{\phi_{j,i}}{\psi_{j,j+1}} \tag{2}$$

where $\phi_{j,i}$ is the angle between jet j and particle i and $\psi_{j,j+1}$ is the angle between jets j and $j+1$. With this definition the four jets have fixed rescaled angle values equal to 0, 1, 2 and 3.

Figure 3a shows the rescaled particle-flow distribution normalised to the number of events after a bin-by-bin background subtraction for the data and MC predictions without CR and for the SKI model with k_{I}=1000, later referred to as SKI 100%. As expected, the latter shows

some depletion in the number of particles in the intra-W regions spanned by the two W bosons (regions A and B) and some particle enhancement in the two inter-W regions (regions C and D) when compared to the model without CR (no-CR).

To improve the sensitivity to CR effects the particle flows in regions A and B are averaged as are the particle flows in regions C and D. The results are shown in Figures 3b and 3c where the angle is redefined to be in the range [0,1]. MC studies at particle level with particles having a momentum greater than 100 MeV show that the CR effects are consistent with the detector level results and have similar magnitudes.

The ratio of the particle flow between the quarks from the same W to that between quarks from different W's is found to be a sensitive observable to cross-talk effects as predicted by the SKI model. These ratios, computed from the particle- and energy-flow distributions at detector level, are shown in Figure 4 for the data, the PYTHIA prediction without CR, the SKI model with k_{I}=3 and SKI 100%.

The differences between the models with and without CR are larger in the middle of the interjet regions. Therefore, in order to quantify the CR effects the ratio R is computed in an interval, $0.2 < \phi_{\mathrm{resc}} < 0.8$, optimized with respect to the sensitivity to SKI 100%. The corresponding variables for particle and energy flow are defined as follows:

$$R_{\mathrm{N}} = \int_{0.2}^{0.8} f_{\mathrm{N}}^{\mathrm{A+B}} \ \mathrm{d}\phi \Big/ \int_{0.2}^{0.8} f_{\mathrm{N}}^{\mathrm{C+D}} \ \mathrm{d}\phi \quad \text{and} \quad R_{\mathrm{E}} = \int_{0.2}^{0.8} f_{\mathrm{E}}^{\mathrm{A+B}} \ \mathrm{d}\phi \Big/ \int_{0.2}^{0.8} f_{\mathrm{E}}^{\mathrm{C+D}} \ \mathrm{d}\phi \tag{3}$$

where, in a region i,

$$f_{\mathrm{N}}^{i} = \frac{1}{N_{\mathrm{evt}}} \frac{\mathrm{d}n}{\mathrm{d}\phi} \quad \text{and} \quad f_{\mathrm{E}}^{i} = \frac{1}{E} \frac{\mathrm{d}E}{\mathrm{d}\phi} \tag{4}$$

The measured values of R_{N} and R_{E} obtained at each centre-of-mass energy are summarised in Table 2. Correlations in the particle rates between the four interjet regions are taken into account by constructing the full covariance matrix. This results in an increase of about 20% of the statistical uncertainty. The values obtained with the complete data sample are:

$$R_{\mathrm{N}} = 0.911 \pm 0.023 \ (\mathrm{stat.})$$
$$R_{\mathrm{E}} = 0.719 \pm 0.035 \ (\mathrm{stat.})$$

An estimate of the sensitivity to the SKI 100% model, shows that R_{N} is 2.6 times more sensitive than R_{E}. Accordingly, the following results and discussion are only based on R_{N}.

Figure 5 shows the measured R_{N} as a function of $\sqrt{s}$ together with PYTHIA no-CR and SKI model predictions. The energy dependence originating from the different pairing purities and jet configurations is in agreement with the model predictions. For the PYTHIA SKI predictions, the ratio decreases with the reconnection probability over the whole energy range with similar magnitude. The data indicate little or no CR.

5 Semileptonic Decays

To verify the quality of the MC simulation of the $\mathrm{W} \to \mathrm{q\bar{q}}$ fragmentation process and the possible biases which may arise when determining the particle yields between reconstructed jets in the detector, the particle- and energy-flow distributions are investigated in $\mathrm{e^+e^-} \to \mathrm{W^+W^-} \to \mathrm{q\bar{q}}l\nu$ where $l = \mathrm{e}, \mu$. For this analysis events are selected with high multiplicity,

large missing momentum and a high energy electron or muon. The missing momentum is considered as a fictitious particle in order to apply the Durham jet algorithm to select 4-jet events with $y_{\rm cut}$=0.01.

The same angular criteria on the four interjet angles as applied in the fully hadronic channel are used here. The purity obtained after selection is about 96% and the efficiency is about 12%. The number of selected semileptonic events is 315 with an expectation of 314.5 events. Particle- and energy-flow distributions are built in a similar way as in the fully hadronic channel with the additional requirement that the charged lepton should be in jet 3 or 4. Figure 6a shows the corresponding particle-flow distribution projected on to the plane of jets 1 and 2 for the data and the KORALW MC prediction. There is good agreement between data and MC over the whole distribution. Figure 6b shows the rescaled particle-flow distribution where the structure of the two different W's is clearly visible. The region between jet 1 and jet 2 corresponds to the hadronically decaying W (W_1) and the region between jet 3 and jet 4 corresponds to the W decaying semileptonically (W_2). The activity in the W_2 region is mainly due to low energy fragments from the hadronic decay of the first W. A comparison of data and MC for the particle flow obtained by summing the regions W_1 and W_2 is shown in Figure 7a. The ratio between the data and the MC distributions is shown in Figure 7b. This ratio is consistent with unity over the whole range. This result gives additional confidence in the correctness of the modelling of the fragmentation process of quark pairs according to the fragmentation parameters used in KORALW and PYTHIA as well as the particle flow definition and reconstruction.

In the absence of CR effects, the activity found in regions A+B of a fully hadronic event should be equivalent to twice the particle activity in the regions W_1+W_2 of the distribution for a semileptonic event. Figure 7c shows the ratio of the particle flow in four-quark events divided by twice the particle flow in semileptonic events for the data and the predictions from no-CR PYTHIA MC and the SKI 100% model. The CR model shows the expected deficit in the hadronic channel compared to the semileptonic one. The data are consistent with the no-CR scheme but the large statistical uncertainty prevents a quantitative statement based on this model-independent comparison.

6 Systematic Uncertainties

Several sources of systematic uncertainties are investigated. The first important test is whether the result depends on the definition of the particles. The analysis is repeated using calorimetric clusters only. Half the difference between the two analyses is assigned as the uncertainty due to this effect. This is found to be the dominant systematic uncertainty.

The second source of systematic uncertainty is the limited knowledge of quark fragmentation modelling. The systematic effect in the $\rm q\bar{q}(\gamma)$ background is estimated by comparing results using the JETSET and HERWIG MC programs. The corresponding uncertainty is assigned to be half the difference between the two models.

The systematic uncertainty from quark fragmentation modelling in W-pair events is estimated by comparing results using PYTHIA, HERWIG and ARIADNE MC samples without CR. The uncertainty is assigned as the RMS between the $R_{\rm N}$ values obtained with the three fragmentation models. Such comparisons between different models test also possible effects of different fragmentation schemes which are not taken into account when varying only fragmentation parameters within one particular model.

Another source associated with fragmentation modelling is the effect of Bose-Einstein correlations (BEC) in hadronic W decays. This effect is estimated by repeating the analysis using

a MC sample with BEC only between particles originating from the same W. An uncertainty is assigned equal to half the difference with the default MC which includes full BEC simulation (BE32 option) [21] in W pairs. The sensitivity of the $R_{\rm N}$ variable to BEC is found to be small.

The third main source of systematic uncertainty is the background estimation. The $q\bar{q}(\gamma)$ background which is subtracted corresponds mainly to QCD four-jet events for which the rate is not well modelled by parton shower programs. PYTHIA underestimates, by about 10%, the four-jet rate in the selected phase space region [22]. A systematic uncertainty is estimated by varying the $q\bar{q}(\gamma)$ cross section by $\pm$ 5% after correcting the corresponding background by +5%. This correction increases the value of $R_{\rm N}$ by 0.004.

A last and small systematic uncertainty is associated with Z-pair production. It is estimated by varying the corresponding cross section by $\pm$ 10%. This variation takes into account all possible uncertainties pertaining to the hadronic channel, from final state interaction effects to the theoretical knowledge of the hadronic cross section.

A summary of the different contributions to the systematic uncertainty is given in Table 3.

The ratio obtained by taking into account the systematic uncertainties is then:

$$R_{\rm N} = 0.915 \pm 0.023\ (\text{stat.}) \pm 0.021\ (\text{syst.})$$

7 Comparison with Models

The $R_{\rm N}$ values predicted by the PYTHIA no-CR, SKI, SKII, ARIADNE no-CR, AR2, HERWIG no-CR and HERWIG CR models are given in Table 4.

The data disfavour extreme scenarios of CR. A comparison with ARIADNE and HERWIG shows that the CR schemes implemented in these two models do not modify significantly the interjet particle activity in the hadronic W-pair decay events. Thus it is not possible to constrain either of these models in the present analysis.

The dependence of $R_{\rm N}$ on the reconnection probability is investigated with the SKI model. For this, four MC samples are used: the no-CR sample and those with $k_{\rm I}$=0.6, 3 and 1000. In the SKI model the fraction of reconnected events is controlled by the $k_{\rm I}$ parameter and the dependence of $R_{\rm N}$ on $k_{\rm I}$ is parametrized as $R_{\rm N}(k_{\rm I}) = p_1(1 - \exp(-p_2 k_{\rm I})) + p_3$ where p_i are free parameters. A χ^2 fit to the data is performed. The χ^2 minimum is at $k_{\rm I} = 0.08$. This value corresponds to about 6% reconnection probability at $\sqrt{s}$=189 GeV. Within the large uncertainty the result is also consistent with no CR effect.

The upper limits on $k_{\rm I}$ at 68% and 95% confidence level are derived as 1.1 and 2.1 respectively. The corresponding reconnection probabilities at $\sqrt{s} = 189$ GeV are 45% and 64%. The extreme SKI scenario, in which CR occurs in essentially all events, is disfavoured by 4.9 σ.

References

[1] G. Gustafson, U. Pettersson and P. Zerwas, Phys. Lett. **B 209** (1988) 90.

[2] T. Sjöstrand and V.A. Khoze, Phys. Rev. Lett. **72** (1994) 28; Z. Phys. **C 62** (1994) 281; V.A. Khoze and T. Sjöstrand, Eur. Phys. J. **C 6** (1999) 271.

[3] G. Gustafson and J. Häkkinen, Z. Phys. **C 64** (1994) 659.

[4] A. Ballestrero et al. in "Physics at LEP2", eds. G. Altarelli et al., CERN 96-01 (1996) 141.

[5] OPAL Collab., K. Ackerstaff *et al.*, Eur. Phys. J. **C 1** (1998) 395; G. Abbiendi *et al.*, Phys. Lett. **B 453** (1999) 153;
DELPHI Collab., P. Abreu *et al.*, Eur. Phys. J. **C 18** (2000) 203; Erratum *ibid.* **C 25** (2002) 493.

[6] D. Duchesneau, preprint LAPP-EXP 2000-02, (2000)
available at http://wwwlapp.in2p3.fr/preplapp/psexp/lappexp0002.ps.gz

[7] L3 Collab, B. Adeva *et al.*, Nucl. Instr. and Meth. **A 289** (1990) 35;
M. Chemarin *et al.*, Nucl. Instr. and Meth. **A 349** (1994) 345;
M. Acciarri *et al.*, Nucl. Instr. and Meth. **A 351** (1994) 300;
G. Basti *et al.*, Nucl. Instr. and Meth. **A 374** (1996) 293;
I. C. Brock *et al.*, Nucl. Instr. and Meth. **A 381** (1996) 236;
A. Adam *et al.*, Nucl. Instr. and Meth. **A 383** (1996) 342.

[8] J. Ellis and K. Geiger, Phys. Rev. **D 54** (1996) 1967.

[9] L. Lönnblad, Z. Phys. **C 70** (1996) 107.

[10] B. Webber, J. Phys. **G 24** (1998) 287.

[11] J. Rathsman, Phys. Lett. **B 452** (1999) 364.

[12] PYTHIA 6.1 Monte Carlo Program:
T. Sjöstrand *et al.*, Comp. Phys. Comm. **135** (2001) 238.

[13] ARIADNE 4.08 Monte Carlo Program:
L. Lönnblad, Comp. Phys. Comm. **71** (1992) 15.

[14] HERWIG 6.2 Monte Carlo Program:
G. Corcella *et al.*, JHEP **01** (2001) 010;
G. Marchesini *et al.*, Comp. Phys. Commun. **67** (1992) 465.

[15] S. Catani *et al.*, Phys. Lett. **B 269** (1991) 432;
N. Brown and W.J. Stirling, Z. Phys. **C 53** (1992) 629;
S. Bethke *et al.*, Nucl. Phys. **B 370** (1992) 310; erratum: ibid. **B 523** (1998) 681.

[16] L3 Collab., P. Achard *et al.*, Phys. Lett. **B 536** (2002) 217.

[17] KORALW 1.42 Monte Carlo Program:
S. Jadach *et al.*, Comp. Phys. Comm. **119** (1999) 272.

[18] KK2F 4.14 Monte Carlo Program:
S. Jadach, B. F. L. Ward and Z. Wąs, Phys. Lett. **B 449** (1999) 97.

[19] JETSET 7.4 Monte Carlo Program:
T. Sjöstrand, preprint CERN-TH-7112/93 (1993), revised 1995;
T. Sjöstrand, Comp. Phys. Comm. **82** (1994) 74.

[20] The L3 detector simulation is based on GEANT Version 3.15.
R. Brun *et al.*, preprint CERN-DD/EE/84-1 (1984), revised 1987.
The GHEISHA program (H. Fesefeldt, RWTH Aachen Report PITHA 85/02 (1985)) is used to simulate hadronic interactions.

[21] L. Lönnblad and T. Sjöstrand, Eur. Phys. J. **C 2** (1998) 165.

[22] A. Ballestrero *et al.*, preprint hep-ph/0006259 (2000).

The L3 Collaboration:

P.Achard,[20] O.Adriani,[17] M.Aguilar-Benitez,[24] J.Alcaraz,[24] G.Alemanni,[22] J.Allaby,[18] A.Aloisio,[28] M.G.Alviggi,[28] H.Anderhub,[46] V.P.Andreev,[6,33] F.Anselmo,[8] A.Arefiev,[27] T.Azemoon,[3] T.Aziz,[9] P.Bagnaia,[38] A.Bajo,[24] G.Baksay,[25] L.Baksay,[25] S.V.Baldew,[2] S.Banerjee,[9] Sw.Banerjee,[4] A.Barczyk,[46,44] R.Barillère,[18] P.Bartalini,[22] M.Basile,[8] N.Batalova,[43] R.Battiston,[32] A.Bay,[22] F.Becattini,[17] U.Becker,[13] F.Behner,[46] L.Bellucci,[17] R.Berbeco,[3] J.Berdugo,[24] P.Berges,[13] B.Bertucci,[32] B.L.Betev,[46] M.Biasini,[32] M.Biglietti,[28] A.Biland,[46] J.J.Blaising,[4] S.C.Blyth,[34] G.J.Bobbink,[2] A.Böhm,[1] L.Boldizsar,[12] B.Borgia,[38] S.Bottai,[17] D.Bourilkov,[46] M.Bourquin,[20] S.Braccini,[20] J.G.Branson,[40] F.Brochu,[4] J.D.Burger,[13] W.J.Burger,[32] X.D.Cai,[13] M.Capell,[13] G.Cara Romeo,[8] G.Carlino,[28] A.Cartacci,[17] J.Casaus,[24] F.Cavallari,[38] N.Cavallo,[35] C.Cecchi,[32] M.Cerrada,[24] M.Chamizo,[20] Y.H.Chang,[48] M.Chemarin,[23] A.Chen,[48] G.Chen,[7] G.M.Chen,[7] H.F.Chen,[21] H.S.Chen,[7] G.Chiefari,[28] L.Cifarelli,[39] F.Cindolo,[8] I.Clare,[13] R.Clare,[37] G.Coignet,[4] N.Colino,[24] S.Costantini,[38] B.de la Cruz,[24] S.Cucciarelli,[32] J.A.van Dalen,[30] R.de Asmundis,[28] P.Déglon,[20] J.Debreczeni,[12] A.Degré,[4] K.Dehmelt,[25] K.Deiters,[44] D.della Volpe,[28] E.Delmeire,[20] P.Denes,[36] F.DeNotaristefani,[38] A.De Salvo,[46] M.Diemoz,[38] M.Dierckxsens,[2] C.Dionisi,[38] M.Dittmar,[46] A.Doria,[28] M.T.Dova,[10,♯] D.Duchesneau,[4] M.Duda,[1] B.Echenard,[20] A.Eline,[18] A.El Hage,[1] H.El Mamouni,[23] A.Engler,[34] F.J.Eppling,[13] P.Extermann,[20] M.A.Falagan,[24] S.Falciano,[38] A.Favara,[31] J.Fay,[23] O.Fedin,[33] M.Felcini,[46] T.Ferguson,[34] H.Fesefeldt,[1] E.Fiandrini,[32] J.H.Field,[20] F.Filthaut,[30] P.H.Fisher,[13] W.Fisher,[36] I.Fisk,[40] G.Forconi,[13] K.Freudenreich,[46] C.Furetta,[26] Yu.Galaktionov,[27,13] S.N.Ganguli,[9] P.Garcia-Abia,[24] M.Gataullin,[31] S.Gentile,[38] S.Giagu,[38] Z.F.Gong,[21] G.Grenier,[23] O.Grimm,[46] M.W.Gruenewald,[16] M.Guida,[39] R.van Gulik,[2] V.K.Gupta,[36] A.Gurtu,[9] L.J.Gutay,[43] D.Haas,[5] R.Sh.Hakobyan,[30] D.Hatzifotiadou,[8] T.Hebbeker,[1] A.Hervé,[18] J.Hirschfelder,[34] H.Hofer,[46] M.Hohlmann,[25] G.Holzner,[46] S.R.Hou,[48] Y.Hu,[30] B.N.Jin,[7] L.W.Jones,[3] P.de Jong,[2] I.Josa-Mutuberría,[24] D.Käfer,[1] M.Kaur,[14] M.N.Kienzle-Focacci,[20] J.K.Kim,[42] J.Kirkby,[18] W.Kittel,[30] A.Klimentov,[13,27] A.C.König,[30] M.Kopal,[43] V.Koutsenko,[13,27] M.Kräber,[46] R.W.Kraemer,[34] A.Krüger,[45] A.Kunin,[13] P.Ladron de Guevara,[24] I.Laktineh,[23] G.Landi,[17] M.Lebeau,[18] A.Lebedev,[13] P.Lebrun,[23] P.Lecomte,[46] P.Lecoq,[18] P.Le Coultre,[46] J.M.Le Goff,[18] R.Leiste,[45] M.Levtchenko,[26] P.Levtchenko,[33] C.Li,[21] S.Likhoded,[45] C.H.Lin,[48] W.T.Lin,[48] F.L.Linde,[2] L.Lista,[28] Z.A.Liu,[7] W.Lohmann,[45] E.Longo,[38] Y.S.Lu,[7] C.Luci,[38] L.Luminari,[38] W.Lustermann,[46] W.G.Ma,[21] L.Malgeri,[20] A.Malinin,[27] C.Maña,[24] J.Mans,[36] J.P.Martin,[23] F.Marzano,[38] K.Mazumdar,[9] R.R.McNeil,[6] S.Mele,[18,28] L.Merola,[28] M.Meschini,[17] W.J.Metzger,[30] A.Mihul,[11] H.Milcent,[18] G.Mirabelli,[38] J.Mnich,[1] G.B.Mohanty,[9] G.S.Muanza,[23] A.J.M.Muijs,[2] B.Musicar,[40] M.Musy,[38] S.Nagy,[15] S.Natale,[20] M.Napolitano,[28] F.Nessi-Tedaldi,[46] H.Newman,[31] A.Nisati,[38] H.Nowak,[45] R.Ofierzynski,[46] G.Organtini,[38] I.Pal,[43] C.Palomares,[24] P.Paolucci,[28] R.Paramatti,[38] G.Passaleva,[17] S.Patricelli,[28] T.Paul,[10] M.Pauluzzi,[32] C.Paus,[13] F.Pauss,[46] M.Pedace,[38] S.Pensotti,[26] D.Perret-Gallix,[4] B.Petersen,[30] D.Piccolo,[28] F.Pierella,[8] M.Pioppi,[32] P.A.Piroué,[36] E.Pistolesi,[26] V.Plyaskin,[27] M.Pohl,[20] V.Pojidaev,[17] J.Pothier,[18] D.Prokofiev,[33] J.Quartieri,[39] G.Rahal-Callot,[46] M.A.Rahaman,[9] P.Raics,[15] N.Raja,[9] R.Ramelli,[46] P.G.Rancoita,[26] R.Ranieri,[17] A.Raspereza,[45] P.Razis,[29] D.Ren,[46] M.Rescigno,[38] S.Reucroft,[10] S.Riemann,[45] K.Riles,[3] B.P.Roe,[3] L.Romero,[24] A.Rosca,[45] S.Rosier-Lees,[4] S.Roth,[1] C.Rosenbleck,[1] J.A.Rubio,[18] G.Ruggiero,[17] H.Rykaczewski,[46] A.Sakharov,[46] S.Saremi,[6] S.Sarkar,[38] J.Salicio,[18] E.Sanchez,[24] C.Schäfer,[18] V.Schegelsky,[33] H.Schopper,[47] D.J.Schotanus,[30] C.Sciacca,[28] L.Servoli,[32] S.Shevchenko,[31] N.Shivarov,[41] V.Shoutko,[13] E.Shumilov,[27] A.Shvorob,[31] D.Son,[42] C.Souga,[23] P.Spillantini,[17] M.Steuer,[13] D.P.Stickland,[36] B.Stoyanov,[41] A.Straessner,[18] K.Sudhakar,[9] G.Sultanov,[41] L.Z.Sun,[21] S.Sushkov,[1] H.Suter,[46] J.D.Swain,[10] Z.Szillasi,[25,¶] X.W.Tang,[7] P.Tarjan,[15] L.Tauscher,[5] L.Taylor,[10] B.Tellili,[23] D.Teyssier,[23] C.Timmermans,[30] Samuel C.C.Ting,[13] S.M.Ting,[13] S.C.Tonwar,[9] J.Tóth,[12] C.Tully,[36] K.L.Tung,[7] J.Ulbricht,[46] E.Valente,[38] R.T.Van de Walle,[30] R.Vasquez,[43] V.Veszpremi,[25] G.Vesztergombi,[12] I.Vetlitsky,[27] D.Vicinanza,[39] G.Viertel,[46] S.Villa,[37] M.Vivargent,[4] S.Vlachos,[5] I.Vodopianov,[25] H.Vogel,[34] H.Vogt,[45] I.Vorobiev,[34,27] A.A.Vorobyov,[33] M.Wadhwa,[5] Q.Wang,[30] X.L.Wang,[21] Z.M.Wang,[21] M.Weber,[1] P.Wienemann,[1] H.Wilkens,[30] S.Wynhoff,[36] L.Xia,[31] Z.Z.Xu,[21] J.Yamamoto,[3] B.Z.Yang,[21] C.G.Yang,[7] H.J.Yang,[3] M.Yang,[7] S.C.Yeh,[49] An.Zalite,[33] Yu.Zalite,[33] Z.P.Zhang,[21] J.Zhao,[21] G.Y.Zhu,[7] R.Y.Zhu,[31] H.L.Zhuang,[7] A.Zichichi,[8,18,19] B.Zimmermann,[46] M.Zöller.[1]

1 III. Physikalisches Institut, RWTH, D-52056 Aachen, Germany§
2 National Institute for High Energy Physics, NIKHEF, and University of Amsterdam, NL-1009 DB Amsterdam, The Netherlands
3 University of Michigan, Ann Arbor, MI 48109, USA
4 Laboratoire d'Annecy-le-Vieux de Physique des Particules, LAPP,IN2P3-CNRS, BP 110, F-74941 Annecy-le-Vieux CEDEX, France
5 Institute of Physics, University of Basel, CH-4056 Basel, Switzerland
6 Louisiana State University, Baton Rouge, LA 70803, USA
7 Institute of High Energy Physics, IHEP, 100039 Beijing, China△
8 University of Bologna and INFN-Sezione di Bologna, I-40126 Bologna, Italy
9 Tata Institute of Fundamental Research, Mumbai (Bombay) 400 005, India
10 Northeastern University, Boston, MA 02115, USA
11 Institute of Atomic Physics and University of Bucharest, R-76900 Bucharest, Romania
12 Central Research Institute for Physics of the Hungarian Academy of Sciences, H-1525 Budapest 114, Hungary‡
13 Massachusetts Institute of Technology, Cambridge, MA 02139, USA
14 Panjab University, Chandigarh 160 014, India.
15 KLTE-ATOMKI, H-4010 Debrecen, Hungary¶
16 Department of Experimental Physics, University College Dublin, Belfield, Dublin 4, Ireland
17 INFN Sezione di Firenze and University of Florence, I-50125 Florence, Italy
18 European Laboratory for Particle Physics, CERN, CH-1211 Geneva 23, Switzerland
19 World Laboratory, FBLJA Project, CH-1211 Geneva 23, Switzerland
20 University of Geneva, CH-1211 Geneva 4, Switzerland
21 Chinese University of Science and Technology, USTC, Hefei, Anhui 230 029, China△
22 University of Lausanne, CH-1015 Lausanne, Switzerland
23 Institut de Physique Nucléaire de Lyon, IN2P3-CNRS,Université Claude Bernard, F-69622 Villeurbanne, France
24 Centro de Investigaciones Energéticas, Medioambientales y Tecnológicas, CIEMAT, E-28040 Madrid, Spain♭
25 Florida Institute of Technology, Melbourne, FL 32901, USA
26 INFN-Sezione di Milano, I-20133 Milan, Italy
27 Institute of Theoretical and Experimental Physics, ITEP, Moscow, Russia
28 INFN-Sezione di Napoli and University of Naples, I-80125 Naples, Italy
29 Department of Physics, University of Cyprus, Nicosia, Cyprus
30 University of Nijmegen and NIKHEF, NL-6525 ED Nijmegen, The Netherlands
31 California Institute of Technology, Pasadena, CA 91125, USA
32 INFN-Sezione di Perugia and Università Degli Studi di Perugia, I-06100 Perugia, Italy
33 Nuclear Physics Institute, St. Petersburg, Russia
34 Carnegie Mellon University, Pittsburgh, PA 15213, USA
35 INFN-Sezione di Napoli and University of Potenza, I-85100 Potenza, Italy
36 Princeton University, Princeton, NJ 08544, USA
37 University of Californa, Riverside, CA 92521, USA
38 INFN-Sezione di Roma and University of Rome, "La Sapienza", I-00185 Rome, Italy
39 University and INFN, Salerno, I-84100 Salerno, Italy
40 University of California, San Diego, CA 92093, USA
41 Bulgarian Academy of Sciences, Central Lab. of Mechatronics and Instrumentation, BU-1113 Sofia, Bulgaria
42 The Center for High Energy Physics, Kyungpook National University, 702-701 Taegu, Republic of Korea
43 Purdue University, West Lafayette, IN 47907, USA
44 Paul Scherrer Institut, PSI, CH-5232 Villigen, Switzerland
45 DESY, D-15738 Zeuthen, Germany
46 Eidgenössische Technische Hochschule, ETH Zürich, CH-8093 Zürich, Switzerland
47 University of Hamburg, D-22761 Hamburg, Germany
48 National Central University, Chung-Li, Taiwan, China
49 Department of Physics, National Tsing Hua University, Taiwan, China
§ Supported by the German Bundesministerium für Bildung, Wissenschaft, Forschung und Technologie
‡ Supported by the Hungarian OTKA fund under contract numbers T019181, F023259 and T037350.
¶ Also supported by the Hungarian OTKA fund under contract number T026178.
♭ Supported also by the Comisión Interministerial de Ciencia y Tecnología.
♯ Also supported by CONICET and Universidad Nacional de La Plata, CC 67, 1900 La Plata, Argentina.
△ Supported by the National Natural Science Foundation of China.

$\langle\sqrt{s}\rangle$ (GeV)	$\mathcal{L}(\mathrm{pb}^{-1})$	N_{events}	N_{MC}	ϵ	π
188.6	176.7	208	226.0	14.2%	88%
191.6	29.7	38	37.9	14.3%	90%
195.5	83.7	104	101.0	13.4%	92%
199.5	84.3	97	91.9	12.2%	93%
201.7	35.5	36	37.2	11.3%	93%
205.1	77.8	75	74.8	10.3%	93%
206.6	138.9	108	120.8	8.9%	91%
198.2	626.6	666	689.6	12.0%	91%

Table 1: Average centre-of-mass energies, integrated luminosities ($\mathcal{L}$), number of selected events (N_{events}), number of expected events (N_{MC}), selection efficiency (ϵ) and percentage of correct jet pairing (π) for the particle flow analysis. The combined figures are given in the last row.

$\langle\sqrt{s}\rangle$ (GeV)	R_{N}	R_{E}
188.6	0.820 ± 0.037	0.610 ± 0.047
191.6	0.929 ± 0.093	0.822 ± 0.133
195.5	0.948 ± 0.059	0.774 ± 0.077
199.5	1.004 ± 0.067	0.871 ± 0.095
201.7	0.770 ± 0.086	0.626 ± 0.130
205.1	1.033 ± 0.083	0.756 ± 0.111
206.6	0.958 ± 0.068	0.781 ± 0.096

Table 2: Measured R_{N} and R_{E} values as a function of energy with their statistical uncertainties.

Source	σ_{R_N}
Energy flow objects	0.016
$q\bar{q}$ fragmentation	0.009
WW fragmentation	0.008
BEC	0.003
4-jet background rate	0.004
ZZ background	0.002
Total	0.021

Table 3: Contributions to the systematic uncertainties on R_N.

	R_N
Data	$0.915 \pm 0.023 \pm 0.021$
PYTHIA no-CR	0.918 ± 0.003
SKI (k_I=0.6)	0.896 ± 0.003
SKI (k_I=3.0)	0.843 ± 0.003
SKI 100%	0.762 ± 0.003
SKII	0.916 ± 0.003
ARIADNE no-CR	0.929 ± 0.003
AR2	0.919 ± 0.003
HERWIG no-CR	0.948 ± 0.005
HERWIG CR	0.946 ± 0.005

Table 4: Measured value of R_N and model predictions.

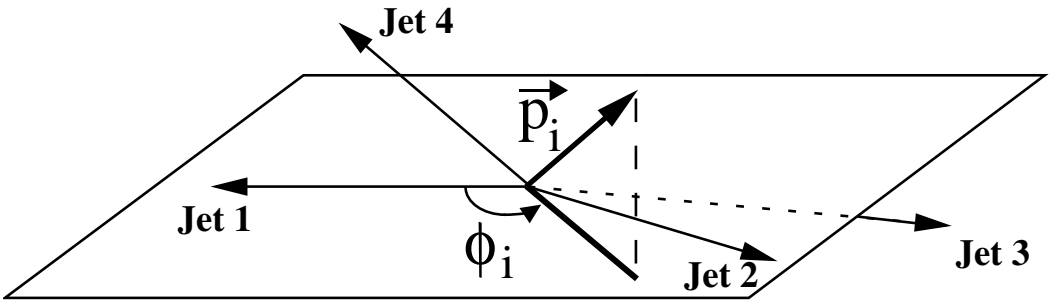

Figure 1: Determination of the ϕ_i angle for the particle i.

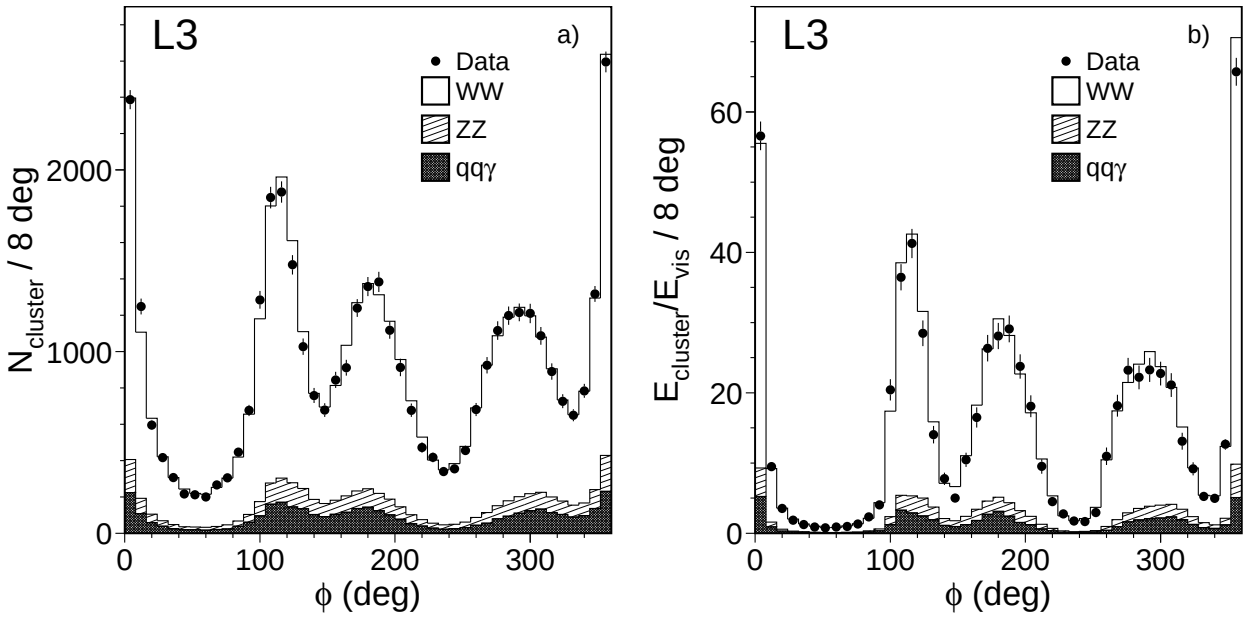

Figure 2: a) Particle- and b) energy-flow distributions at $\sqrt{s} = 189 - 209$ GeV for data and MC predictions.

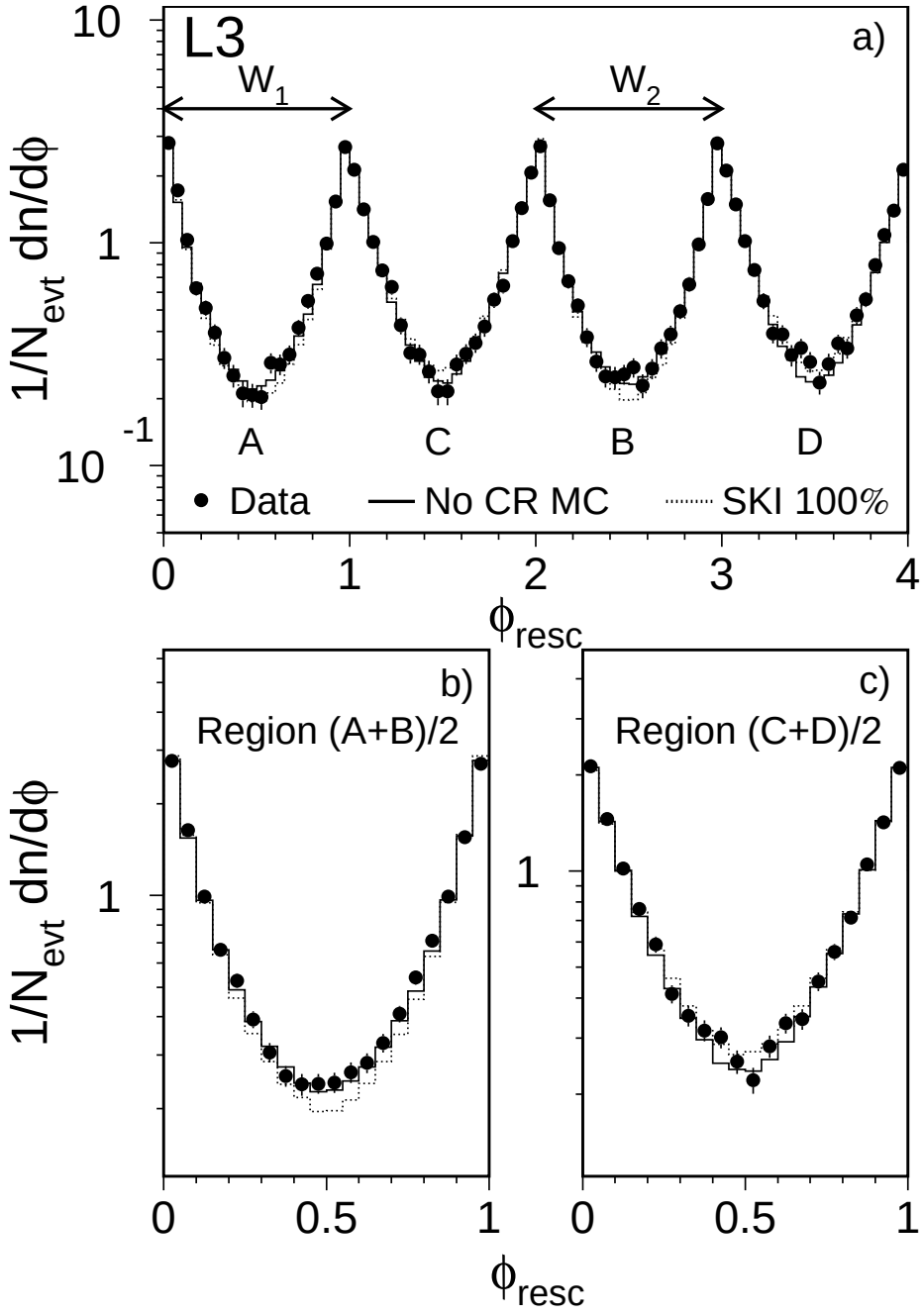

Figure 3: a) Particle-flow distribution as a function of the rescaled angle for data and for PYTHIA MC predictions without CR, and with the SKI 100% model. Distributions of b) combined intra-W particle flow and c) combined inter-W particle flow.

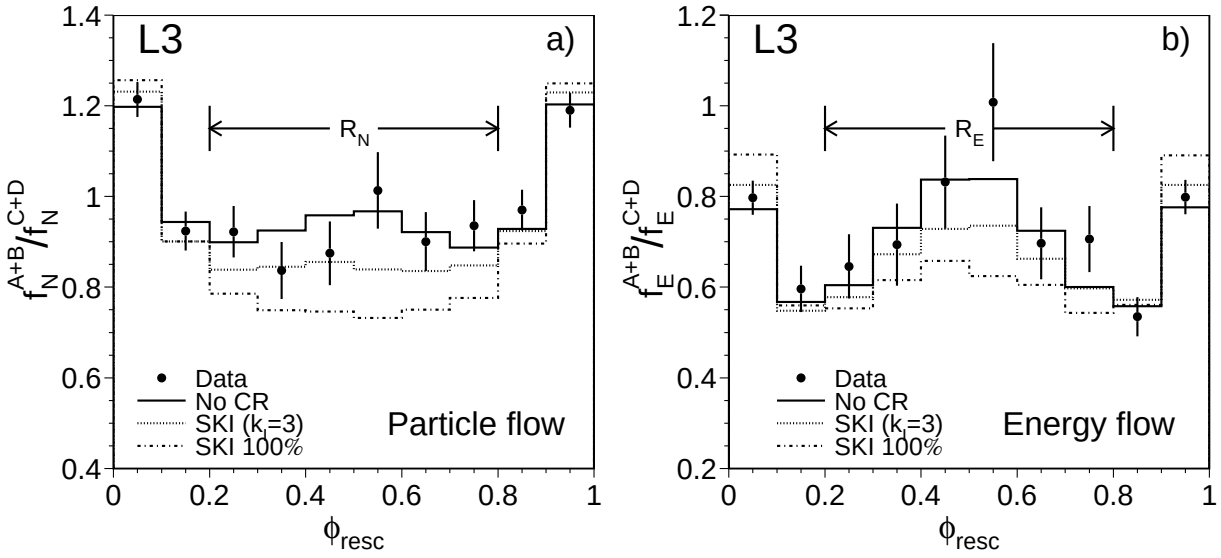

Figure 4: Ratio of a) particle- and b) energy-flow distributions (Equation 4) in regions A+B to that in regions C+D. Statistical uncertainties are shown.

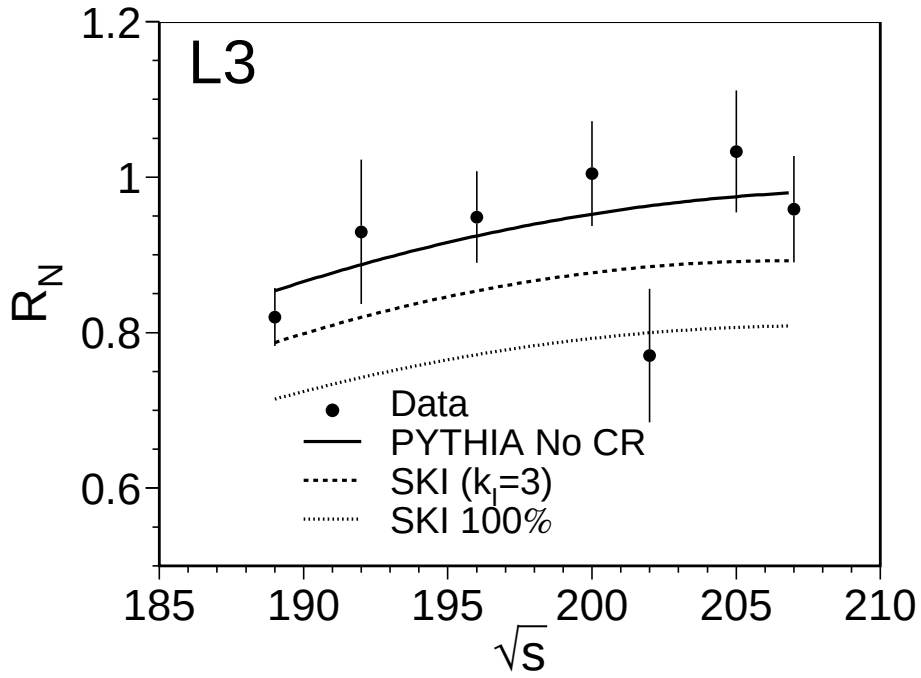

Figure 5: The ratio $R_{\rm N}$ as a function of $\sqrt{s}$ at detector level for data and PYTHIA no-CR and SKI model predictions. The parametrisation of the energy dependence is obtained by fitting a second order polynomial function to the predicted MC dependence. The parametrisation obtained with PYTHIA no-CR gives $R_{\rm N}(\sqrt{s})/R_{\rm N}(189\,{\rm GeV}) = -3.07\times10^{-4}s+0.1297\sqrt{s}-12.56$. The dependence obtained with the SKI model ($k_{\rm I}$= 3) leads to a 2.3% change in the average rescaled $R_{\rm N}$ value at 189 GeV.

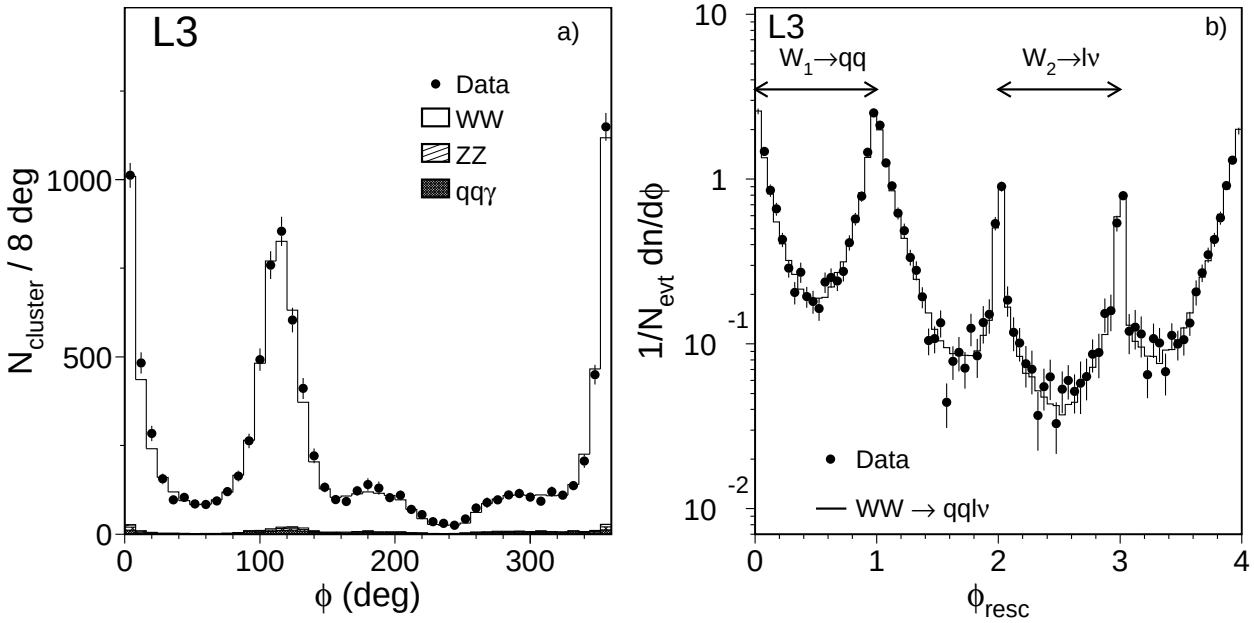

Figure 6: Particle-flow distributions a) before and b) after angle rescaling for the semileptonic W decays for data and KORALW prediction.

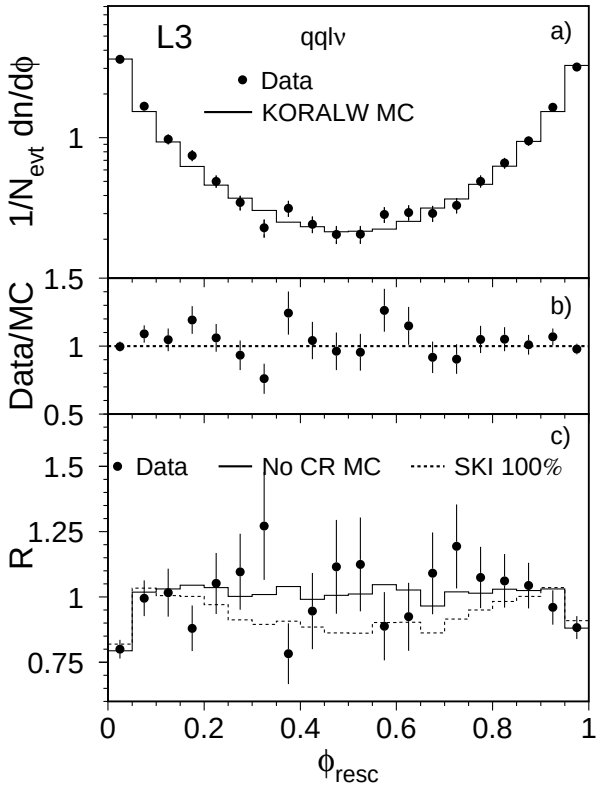

Figure 7: a) Particle-flow distributions as a function of the rescaled angle for the semileptonic W decays for data and the KORALW prediction. b) Ratio of data and MC as a function of the rescaled angle. c) Ratio R of the particle flow in hadronic events divided by twice the particle flow in semileptonic events.